

The effect of CO₂ on the speciation of bromine in low-temperature geological solutions: an XANES study

K. A. Evans,^{a*} J. Mavrogenes^a and M. Newville^b

^aResearch School of Earth Sciences, Australian National University, Canberra, ACT 0200, Australia, and ^bGSECARS, APS, Argonne National Laboratory, 9700 South Cass Avenue, Building 460, Argonne, IL 60439, USA. E-mail: katy.evans@anu.edu.au

Received 31 October 2006

Accepted 10 January 2007

CO₂-rich solutions are common in geological environments. An XANES (X-ray absorption near-edge structure) study of Br in CO₂-bearing synthetic fluid inclusions has revealed that Br exhibits a strong pre-edge feature at temperatures from 298 to 423 K. Br in CO₂-free solutions does not show such a feature. The feature becomes smaller and disappears as temperature increases, but reappears when temperature is reduced. The size of the feature increases with increasing $X(\text{CO}_2)$ in the fluid inclusion, where $X(\text{CO}_2)$ is the mole fraction of CO₂ in the solution [$n_{\text{CO}_2}/(n_{\text{CO}_2} + n_{\text{H}_2\text{O}} + n_{\text{RbBr}})$; n indicates the number of moles]. The pre-edge feature is similar to that shown by covalently bonded Br, but observed and calculated concentrations of plausible Br-bearing covalent compounds (Br₂, CH₃Br and HBr) are vanishingly small. An alternative possibility is that CO₂ affects the hydration of Br sufficiently that the charge density changes to favour the $1s \rightarrow p$ level transitions that are thought to cause the pre-edge peak. The distance between the first two post-edge maxima in the XANES also decreases with increasing $X(\text{CO}_2)$. This is attributed to a CO₂-related decrease in the polarity of the solvent. The proposed causes of the observed features are not integrated into existing geochemical models; thus CO₂-bearing solutions could be predicted poorly by such models, with significant consequences for models of geological processes such as ore-formation and metamorphism.

© 2007 International Union of Crystallography
Printed in Singapore – all rights reserved

Keywords: XANES; RbBr; CO₂; XAS.

1. Introduction

CO₂ and dissolved salts such as NaCl are common components of solutions in the earth's crust (Fyfe *et al.*, 1978). The presence of CO₂ affects solution properties such as viscosity and boiling point which in turn affect the ability of solutions to dissolve minerals and metals (Walther, 1992). Few studies have addressed these effects, partly because of the difficulty of containing and observing CO₂-bearing fluids at the pressures and temperatures found in the earth's crust.

This work used XAFS (X-ray absorption fine structure) spectra of synthetic fluid inclusions (SFLINCS) to study the characteristics of CO₂-bearing fluids at elevated pressures and temperatures. SFLINCS are samples of fluids of known composition that have been trapped inside quartz crystals in the laboratory at the pressures and temperatures of interest (Sterner & Bodnar, 1991; Bodnar, 1994). These inclusions provide an artificial environment that, when heated, exposes the fluids to the pressures at which they were created. The absorption edges of Na and Cl, constituents of the most

common salt in geological solutions, lie at such low energies that absorption by the host quartz crystal removes >99% of the XAFS signal from a SFLINC. For this reason, RbBr, which has much higher energy absorption edges, was used as an analogue.

RbBr dissolved in CO₂-free aqueous solution has been the subject of previous work (*e.g.* Fulton *et al.*, 1996; Wallen *et al.*, 1997; Ferlat *et al.*, 2002; Filippini *et al.*, 2003). An aim of some of these studies was to determine whether ion association increases as a function of increasing ionic strength and pressure, but results have been ambiguous. The presence of CO₂ is also expected to increase the probability of ion association because it decreases the dielectric constant of solutions, but this is the first study to use solutions that contain both a salt and CO₂. The aim of the study was, therefore, to determine whether CO₂-induced changes in the structure of the solution can be measured by XAFS. An unexpected and previously unobserved result of the study was the presence of a pre-edge XANES (X-ray absorption near-edge structure) feature on the Br edge for CO₂-bearing solutions. Here, the nature of this

Table 1

Summary of sample compositions.

P: pressure. *T*: temperature. *X*(CO₂) and *X*(RbBr) are the mole fractions of CO₂ and RbBr, respectively. N/A: not applicable.

Sample	CO ₂ source	<i>P</i> (kbar)	<i>T</i> (K)	<i>X</i> (CO ₂)	<i>X</i> (RbBr)	Phases†
KRB2	N/A	2.5	1073	0	0.01	L, WV
KRB5	AgOx	2.5	1073	0.02	0.01	L, WV
KRBC10	Oxal	5	1073	0.13	0.008	L, WV, CV
KRBC11	AgOx	5	1073	0.43	0.009	L, WV, CV
KRBC14	AgOx	5	1073	0.09	0.078	L, WV, CV, Cl

† L: liquid. WV: water vapour. CV: CO₂ vapour. Cl: crystal.

feature, possible reasons for it, and the implications that the observations have for natural processes are discussed.

2. Methods

Pre-cracked quartz was loaded into 5 mm-diameter Pt tubing with weighed quantities of RbBr, water and a CO₂ source. Compositions are summarized in Table 1. The CO₂ source was silver oxalate in all cases except KRBC10, for which oxalic acid was used. The Pt tubes were sealed by welding and heated for an hour or two to check for leaks, before being loaded into the cold-seal apparatus at the Department of Earth and Marine Sciences, Australian National University. Samples KRB2 and KRB5 were run for one week at 1073 K and 2.5 kbar. Samples KRBC10, 11 and 14 were run at 1073 K and 5 kbar for 1 week. Oxygen fugacity was buffered to around Ni/NiO by the Ni-rich alloys from which the cold-seal apparatus is constructed (Matthews *et al.*, 2003). After the run the quartz was extracted, set into EPO-FIX epoxy and double polished to approximately 1 mm thickness. The crystals were then removed from the epoxy. Phases present were identified by optical examination. Further characterization was performed using microthermometry and IR (infra-red) microscopy techniques (Table 2).

XANES measurements were made at the GSE-CARS 13-ID beamline at the APS (Advanced Photon Source, Chicago, USA). The energy of incident radiation was controlled using a Si(111) double-crystal monochromator with an energy resolution of around 0.1 eV. The monochromator was slightly detuned to enhance rejection of harmonics. The fluorescent signal was detected with a Vortex Si-drift detector. All samples, including the standards, were measured in fluorescence geometry. The double-polished quartz chips were loaded on a high-temperature LINKAM heating stage (TS1500) at GSE-CARS. XAFS scans were made across the Br edge (13474 eV) from 100 eV before to 400 eV after the edge. Three scans were made at each location to increase the statistical quality of the data. The samples were heated at 50 K min⁻¹ to the temperature of interest and held there for at least half an hour before beginning measurement to allow heating-related sample expansion/contraction to cease. The beam was defocused to around 30 µm diameter so that it covered the whole of the fluid inclusion under examination. Thus, the signal incorporates information from both the liquid

Table 2

Summary of microthermometric and IR spectroscopic results.

*T*_{h1}: temperature at which the double bubble goes to a single bubble. *T*_{h2}: temperature of total homogenization. *T*_{clathmelt}: temperature of clathrate melting. *T*_{firstmelt}: temperature of first ice melt. *T*_{finalmelt}: temperature of melting of last bit of ice. N/A: not applicable. N/D: not determined.

Sample	<i>T</i> _{h1} (K)	<i>T</i> _{h2} (K)	<i>T</i> _{clathmelt} (K)	<i>T</i> _{firstmelt} (K)	<i>T</i> _{finalmelt} (K)	Compounds detected by IR
KRB2	N/A	628.7	N/A	260.7	N/D	N/D
KRB5	N/A	613–633	N/A	261	N/D	N/D
KRBC10	305.1	656.5	223.4	257.8	272.8	H ₂ O, CO ₂
KRBC11	292.5	668.5	228.4	N/A	N/D	H ₂ O, CO ₂
KRBC14	281.4	>703	220	259.4	272	N/D

and the vapour at temperatures less than the homogenization temperature. However, given the relative densities of the two phases, it is likely that the bulk of Br was found in the liquid phase.

Standard solutions, which included solutions with an *X*(RbBr) of 0.01 and 0.001, and saturated NaHCO₃, Na₂CO₃ and K₂CO₃ with 5 molal RbBr, were measured at room temperature. The carbonate solutions were used to provide a CO₂-bearing standard, although the high pH and high ionic strength of these solutions gives them quite different characteristics to the circumneutral solutions of much lower ionic strength that were contained in the SFLINCS.

The spectra were processed using the *Athena* and *Artemis* software packages (Ravel & Newville, 2005). The first derivative of the spectra was used to determine the positions of the first few maxima and minima for each spectrum (Fig. 1, Table 3). If a pre-edge peak was present then five points were measured, where the first two points describe the pre-edge peak. If no pre-edge peak was measured then only three

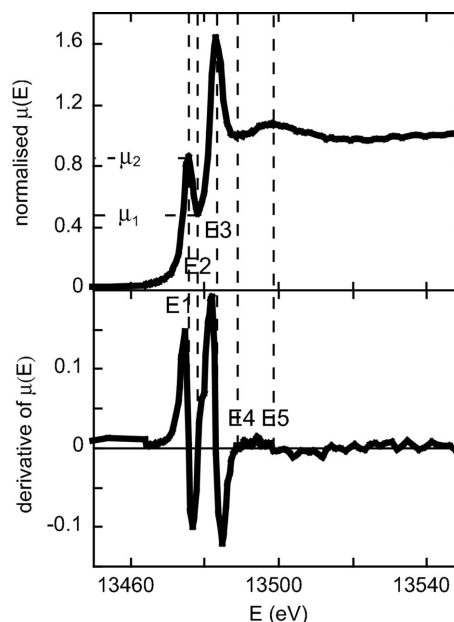


Figure 1
Location of the points used to characterize the XANES spectra.

Table 3

Characteristics of the pre-edge peak.

N/A: not applicable.

Sample	$X(\text{CO}_2)$	T (K)	E_1	E_2	E_3	E_4	E_5	Inflection	$E_5 - E_3$	$\mu(E)_1$	$\mu(E)_2$	$\Delta\mu(E)$
KRB2	0	298	N/A	N/A	13482.08	13489.63	13499.96	N/A	17.88	N/A	N/A	N/A
KRB5	0.01	298	N/A	N/A	13481.61	13489.63	13499.09	N/A	17.48	N/A	N/A	N/A
KRBC11	0.43	298	N/A	N/A	13483.11	13489.63	13496.62	13477.1	13.51	N/A	N/A	N/A
KRBC10	0.13	373	13476.2	13478.6	13482.56	13488.59	13495.99	N/A	13.43	0.71	1.23	0.52
KRBC10	0.13	423	13476.53	13477	13482.56	13489.07	13498.53	N/A	15.97	1.54	1.56	0.02
KRBC10	0.13	423	N/A	N/A	13481.6	13489.1	13499.1	N/A	17.5	N/A	N/A	N/A
KRBC10	0.13	373	13476	13478.6	13482.56	13488.12	13497.1	N/A	14.54	0.49	N/A	N/A
KRBC10	0.13	423	13476.6	13477	13482.08	13489.63	13499.96	N/A	17.88	0.46	N/A	N/A
KRBC10	0.13	298	13475.9	13478.7	13482.56	13487.56	13495.51	N/A	12.95	0.39	0.73	0.34
KRBC14	0.09	413	N/A	N/A	13482.08	13489.07	13499.09	13477	17.01	N/A	N/A	N/A
KRBC14	0.09	433	N/A	N/A	13482.08	13489.07	13499.09	13476.6	17.01	N/A	N/A	N/A
KRBC14	0.09	298	13476.6	13478.4	13483.11	13489.07	13499.09	N/A	15.98	0.62	0.86	0.24
KRBC14	0.09	298	13476.3	13478.5	13483.11	13489.07	13499.09	N/A	15.98	0.61	0.9	0.29
KRBC14	0.09	373	N/A	N/A	13482.56	13489.07	13498.53	13477.1	15.97	0.5	0.52	0.02
KRBC14	0.09	348	13476.6	13478.8	13482.56	13489.63	13498.53	N/A	15.97	0.75	0.83	0.08
KRBC14	0.09	363	13476.9	13477.8	13482.56	13489.63	13499.96	N/A	17.4	0.92	0.95	0.03
KRBC14	0.09	373	N/A	N/A	13482.56	13489.07	13499.96	13477.2	17.4	1.11	1.11	0
KRBC14	0.09	383	N/A	N/A	13482.08	13489.07	13499.09	13477	17.01	N/A	N/A	N/A
KRBC14	0.09	393	N/A	N/A	13482.08	13489.07	13501	13476.8	18.92	N/A	N/A	N/A
KRBC14	0.09	423	N/A	N/A	13482.08	13489.63	13499.09	N/A	17.01	N/A	N/A	N/A

points were measured, which are equivalent to the third, fourth and fifth points for the samples with the pre-edge peak.

3. Results

CO_2 -free fluid inclusions contained liquid and vapour at low $X(\text{RbBr})$, and liquid, vapour and cubic crystals, inferred to be RbBr, at high $X(\text{RbBr})$. CO_2 -bearing fluid inclusions contained liquid and a double vapour bubble which merged to a single vapour bubble at temperatures close to room temperature (T_{h1}). CO_2 -bearing fluid inclusions with a high $X(\text{RbBr})$ also contained one or two crystal phases, one cubic (common) and a rarer acicular phase. Acicular crystals were only observed in very highly saline inclusions, none of which were analysed for this study. Microthermometry results for KRBC10, 11 and 14 are consistent with CO_2 -bearing ($T_{\text{clathmelt}}$ close to 217 K; Table 2) and RbBr-bearing ($T_{\text{firstmelt}}$ close to 258 K; Table 2) solutions. These results are supported by the IR spectroscopy measurements, which identified H_2O and CO_2 (Table 2). No other compounds were identified.

XANES spectra from SFLINCS with an $X(\text{CO}_2)$ of more than 0.02 and less than 0.2 show a pre-edge feature at temperatures below 423 K whereas spectra from CO_2 -free SFLINCS do not (Fig. 2a). The pre-edge feature is not observed in either the standard RbBr solution or the carbonate-bearing solutions. The pre-edge feature is identical for inclusions within the same sample (Fig. 2b), and decreases in size with increasing temperature (Fig. 2c), finally vanishing before 423 K. Cooling the fluid inclusion resulted in the reappearance of the pre-edge feature (Fig. 2d). The temperature at which the feature disappeared was different for KRBC10 and KRBC14 (Fig. 2e), and, for the limited sample set here, the temperature of the peak disappearance increased with $X(\text{CO}_2)$ (Fig. 2e). The highest $X(\text{CO}_2)$ sample [KRBC11: $X(\text{CO}_2) = 0.495$, Fig. 2f] exhibits only a small pre-

edge feature that looks different to the more defined feature in the lower $X(\text{CO}_2)$ samples. The spectra also show a white line that is much more intense than that observed for the lower $X(\text{CO}_2)$ samples.

$E_5 - E_3$ and $\mu(E)_2 - \mu(E)_1$ exhibit trends as a function of $X(\text{CO}_2)$ and temperature (Fig. 3, Table 3). The most pronounced trend is the decrease in $E_5 - E_3$ at room temperature as a function of $X(\text{CO}_2)$ (Fig. 3a). $E_5 - E_3$ shows little relationship with temperature (Fig. 3b). $\mu(E)_2 - \mu(E)_1$ increases with $X(\text{CO}_2)$ for any given temperature (Fig. 3c: R at 278 K = 0.87, R at 278 K < T < 373 K = 0.97), and decreases with temperature for any given $X(\text{CO}_2)$ [Fig. 3d: R at $X(\text{CO}_2)$ of 0.09 is 0.99, R at $X(\text{CO}_2)$ of 0.13 is 0.65].

4. Discussion

Pre-edge peaks in Br K -edge spectra are attributed to the transition between the $1s$ core level to an unfilled bound p state (Burattini *et al.*, 1991). Br compounds in which the Br is covalently bound exhibit such pre-edge features (*e.g.* Burattini *et al.*, 1991; D'Angelo *et al.*, 1993; Ascone *et al.*, 1994; Filipponi & D'Angelo, 1998; Feiters *et al.*, 2005) but hydrated Br in electrolyte solutions, and Br in solid RbBr, do not (*e.g.* Wallen *et al.*, 1997; Feiters *et al.*, 2005). It is therefore possible that some of the Br at temperatures lower than 423 K is hosted by a covalently bonded compound. The strength of the pre-edge peak depends on the polarity of the solvent. Burattini *et al.* (1991) observe that pre-edge peaks are enhanced and that the distance between the first two post-edge peaks ($E_5 - E_3$) decreases in low-polarity solvents such as hexane. The link between the presence of the pre-edge peak and solvent polarity is supported by the lack of pre-edge peak in the high-ionic-strength carbonate standard solutions.

The decrease in $E_5 - E_3$ with $X(\text{CO}_2)$ (Fig. 3a) suggests that the polarity of the solvent decreases significantly as a result of

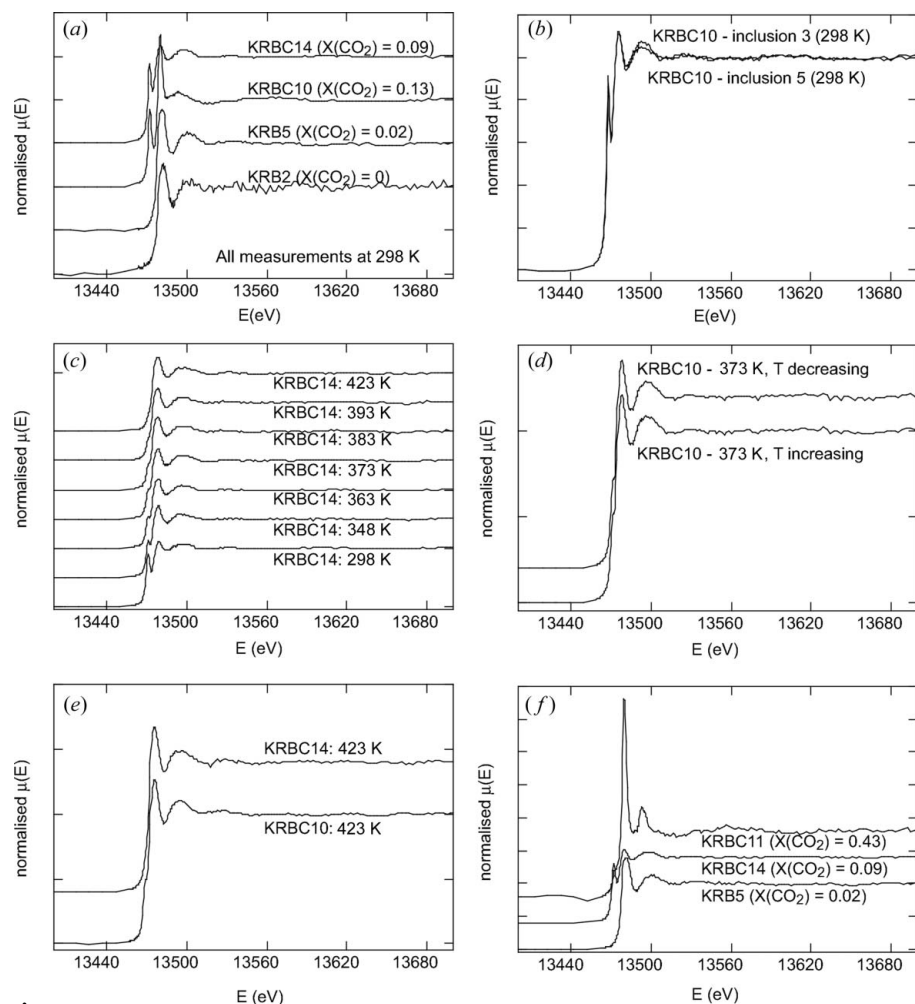


Figure 2
 Characteristics of the XANES spectra. Spectra are offset for clarity. Standard solutions are not shown. (a) CO₂-bearing solutions show a pre-edge peak not shown by the CO₂-free solutions. (b) The pre-edge peak is identical for SFLINCS within a sample (small differences in amplitude are likely to be due to changes in self absorption with inclusion depth). (c) The pre-edge peak decreases in size and then disappears as temperature increases. (d) Cooling the fluid results in the appearance of the pre-edge feature at the same temperature as that at which it disappeared. The cause of the peak is therefore not affected by kinetic factors. (e) The pre-edge peak is of different magnitude in samples with different $X(\text{CO}_2)$: in KRBC14 [$X(\text{CO}_2) = 0.09$] the peak has vanished by 423 K whereas in KRBC10 [$X(\text{CO}_2) = 0.13$] an inflection is still visible. (f) The highest $X(\text{CO}_2)$ sample (KRBC11) shows a significantly different XANES spectra with only a small pre-edge peak.

the presence of CO₂. $E_5 - E_3$ is not sensitive to temperature (Fig. 3b), which suggests that the effect of CO₂ on solvent polarity is not affected much by temperature. The link between the presence of CO₂ and the peak, and the increase in peak size with increasing $X(\text{CO}_2)$ (Fig. 3c) suggests that the presence of CO₂ is related to the cause of the pre-edge peak, either directly, *via* C- and Br-bearing compounds, or indirectly, *via* its effect on the solution chemistry. The decrease and eventual disappearance of the peak with increasing temperature suggests that the cause of the peak becomes less effective with increasing temperature.

Other evidence that can be used to deduce possible sources of the pre-edge peak include consideration of the relative electronegativities of the elements in the system and results of thermodynamic simulation of the system.

4.1. Electronegativity

Covalent bonding is favoured between elements that have similar electronegativities. The greater the difference in electronegativity, the greater the dipole moment and hence the ionic character of the bond (Brownlow, 1979). Electronegativities of the elements present in the experimental system are summarized in Table 4, and the combined electronegativity and bond lengths of potential bonds are summarized in Table 5. Bonds known to give pre-edge features (Br–Br: D’Angelo *et al.*, 1993; H–Br: D’Angelo *et al.*, 1993; Br–C: Burattini *et al.*, 1991) have combined electronegativities of less than 0.7. Ag–Br must also be considered, as Ag sourced from the silver oxalate is also present in the system. The Ag–Br bond has an electronegativity of 0.9 and does not show a pre-edge feature (di Cicco *et al.*, 2000). It is not known whether the bromate ion displays a pre-edge peak; the electronegativity of the bond is low so the bond might be expected to show a pre-edge feature although the electronegativity may be misleading as Br acts as a cation in bromate. H–Br, Br–Br and C–Br bonds would be favoured by a reducing environment [low Eh (redox potential)] while Br–O (bromate) is favoured by an oxidizing (high Eh) environment. The absolute abundance of oxygen is not a control on the type of Br complex that forms, as ample oxygen is present in the water in solution to form bromate when Eh conditions are appropriate.

The ability of oxidation state to control the identity of the Br-bearing complex necessitates consideration of the effect of the Ni/NiO oxygen buffer on the SFLINCS contents.

4.2. Thermodynamic simulation: effect of Ni/NiO buffering

Four-phase (L + V1 + V2 + C1 + Q; *e.g.* KRBC14) and five-phase (L + V1 + V2 + C1 + C2 + Q; KRB19) assemblages are univariant and invariant, respectively, in the four-component system RbBr, H₂O, quartz and Ag₂C₂O₄. The occurrence of such low-variance assemblages suggests that the system comprised more than four components during equilibration and formation of the fluid inclusions. The most likely cause for this is movement of hydrogen through the walls of the platinum capsule (Chou *et al.*, 1978). If hydrogen was mobile

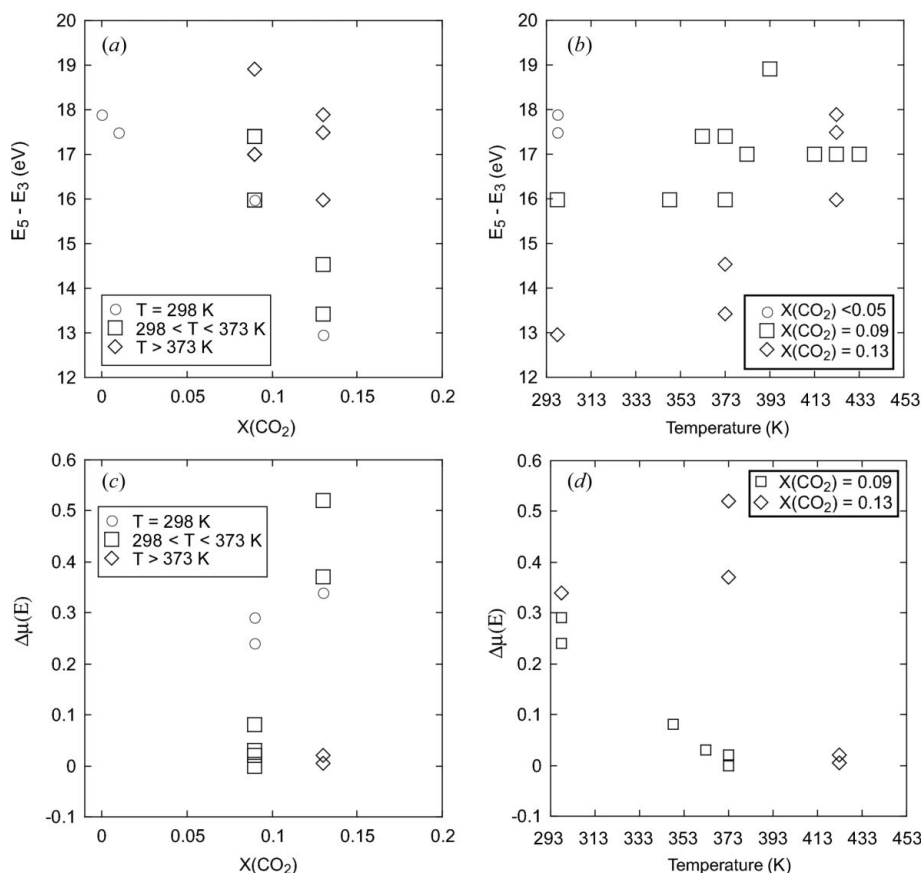


Figure 3 Characteristics of the first derivative of the XANES spectra. (a) $E_5 - E_3$ decreases with increasing $X(\text{CO}_2)$; this indicates a decrease in solvent polarity. (b) $E_5 - E_3$, unaffected by temperature. (c) $\Delta\mu$, which reflects the size of the pre-edge peak, increases with $X(\text{CO}_2)$ for any given temperature. (d) $\Delta\mu$ decreases with increasing temperature for any given $X(\text{CO}_2)$.

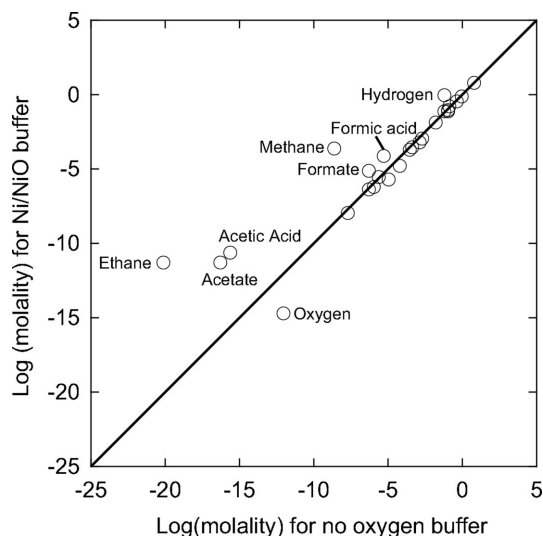


Figure 4 Comparison between the molality of selected species calculated for SFLINCS that experienced no hydrogen diffusion (x axis), and for SFLINCS on the Ni/NiO oxygen buffer (y axis). Unlabelled species are insensitive to redox conditions. Buffering by Ni/NiO causes an increase in the concentration of reduced carbon-bearing species, and a decrease in the concentration of oxygen relative to the unbuffered situation.

Table 4 Element electronegativities (Pauling scale).

Element	Electronegativity
Br	2.8
H	2.1
Ag	1.9
Rb	0.8
C	2.5
O	3.44

then the oxygen fugacity of the system would have been set by the cold-seal apparatus to around Ni/NiO (Matthews *et al.*, 2003). Quenching is almost instantaneous, so the fluid inclusion is unlikely to have undergone electron transfer after this time. The availability of electrons within the fluid inclusion, which is measured by the redox budget (Evans, 2006), is, therefore, likely to have been fixed by equilibration with Ni/NiO at the peak pressure and temperature.

The effect of hydrogen diffusion was investigated using the geochemical modelling program *HCh* (Shvarov & Bastrakov, 1999). The system investigated was C–O–H–NaCl–Ag because high-*PT* thermodynamic data for RbBr are unavailable. Thus, calculated concentrations are incorrect but trends should be comparable with those for the RbBr-bearing experimental system.

Data for halogenated hydrocarbons were also unavailable, but methane and ethane were present in the database, so the presence of methane and ethane was taken to imply that halogenated hydrocarbons may also have been present. The equilibrium distribution of species was calculated for a fluid with the composition of KRBC10 at 1073 K and 0.5 GPa (a) without an oxygen buffer and (b) with oxygen fugacity buffered by Ni/NiO (Fig. 4). The equilibrium distribution of species, rather than a simple comparison of Eh values, was calculated, because knowledge of this distribution is necessary to determine whether significant quantities of reduced hydrocarbon were produced by equilibration with the Ni/NiO buffer.

Calculated concentrations of carbon-bearing species, oxygen and hydrogen differed between the two calculations (Fig. 4). Equilibration with the Ni/NiO buffer increases the concentration of relatively reduced species such as methane, ethane, acetate and formic acid at the expense of oxidized species such as oxygen. The extent of this reduction was calculated. The redox budget of the unbuffered fluid, relative to C(+4), H(+) and O(−2) and Ag(0), was zero, as expected, whereas the redox budget of the buffered fluid relative to the same reference state was −2.01 moles per kg of solution. This is sufficient to convert up to 5% of the CO_2 -hosted carbon in

Table 5

Combined electronegativities (Pauling scale) and bond lengths for Br-bearing bonds.

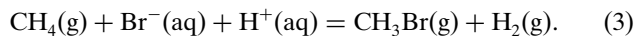
Bond	Electro-negativity	Bond length	Comment
Br–Br	0	2.28	Known to show pre-edge†
H–Br	0.7	1.41	Known to show pre-edge†
Ag–Br	0.9	2.87	Solid and melt do not show covalent bonding‡
Rb–Br	2	3.43	Definitely ionic
C–Br	0.3	1.94	Covalent with pre-edge in some compounds§
Br–O	0.6	1.65¶	Bromate spectra unavailable but may show pre-edge

† Filliponi & D'Angelo (1998). ‡ di Cicco *et al.* (2000). § Burattini *et al.* (1991). ¶ Levason *et al.* (1990).

the fluid inclusion to reduced hydrocarbon-hosted carbon. It is therefore unlikely that bromate, which requires oxidizing conditions, was stabilized by the reaction.

4.3. Thermodynamic simulation: room temperature

Bromine in HBr(g), Br₂(g) and CH₃Br(g) exhibits pre-edge peaks, so it is useful to consider the probability of their presence. The relative stabilities of HBr(g), Br₂(g) and CH₃Br(g) at room temperature can be considered *via* equations (1)–(3),



Stability constants for these reactions were calculated using the thermodynamic data in Table 6, and were rearranged to give the activity of the gas species of interest at room temperature as a function of the activities of the other species [equations (4)–(6)],

$$\ln[HBr] = -21.7 + \ln[Br^-] - 2.303 \text{ pH},$$

$$\ln[Br_2] = -93 + 2 \ln[Br^-] - \ln[H_2] - 4.606 \text{ pH},$$

$$\ln[CH_3Br] = -88.7 + \ln[Br^-] - \ln[H_2] - 2.303 \text{ pH} + \ln[CH_4].$$

The range of possible maximum activities of each of the three species was then calculated as a function of the hydrogen activity by assuming (a) that the activity of Br[−] was the maximum possible concentration (0.6 molal for KRBC10), (b) that pH was between 1 and 10, and (c) that the activity of CH₄ in the gas phase was 0.001; microthermometrical and IR observations did not identify CH₄, but mole fractions of up to 0.001 could have been overlooked by these techniques. Plots of the possible activities (Fig. 5) show that none of the possible species are likely to be present in quantities sufficient to produce a noticeable pre-edge feature for any plausible activity of hydrogen in the gas. All three species partition strongly into the gas phase so significant concentrations of dissolved Br₂, CH₃Br and HBr are also unlikely.

Table 6

Thermodynamic properties used for room-temperature calculations.

Species	$\Delta_f G_{298.1}^\ominus$ (kJ mol ^{−1})	Source
H ₂ (g)	0	Lide (2000)
H ⁺ (aq)	0	Lide (2000)
Br [−] (aq)	−102.8	http://www.ualberta.ca/~jplambec/che/data/p00404.htm
Br ₂ (g)	3.14	Lide (2000)
HBr(g)	−53.5	Lide (2000)
CH ₄ (g)	−124.8	Lide (2000)
CH ₃ Br(g)	−26.3	Lide (2000)

4.4. Alternatives

Br[−] ions in CO₂-free solutions are surrounded by a solvation shell of water molecules which are hydrogen-bonded to the surrounding H₂O network (Grossfield, 2005). CO₂ breaks up the hydrogen-bonded network and reduces the polarity of the solution, as indicated by the decrease in *E*₅ − *E*₃ shown in Fig. 3(a). It is likely that this disturbance of the hydrogen-bonded network affects ion hydration and, consequently, the charge distribution around the ion. One effect of this might be to favour 1s to *p* level transitions that can cause the observed pre-edge peak. The disappearance of the pre-edge feature with increasing temperature is reasonable for a feature caused by changes in hydrogen bonding; hydrogen bonding decreases in strength and effectiveness as temperature increases (Jorgensen & Madura, 1985).

A further possibility is the presence of intermolecular bonding that involves elements other than hydrogen. Intermolecular bonds are represented by *D* · · · *X*–*Y* (*e.g.* Metrangolo *et al.*, 2005) where *D* is an electron donor or acceptor and *X*–*Y* is a molecule with an asymmetric charge distribution. Intermolecular bonding distorts the charge distribution around ions and could, therefore, facilitate the 1s–*p* level transition thought to cause the pre-edge feature. Hydrogen bonding is the best known form of intermolecular bonding, halogen bonding is another (*e.g.* Metrangolo & Resnati, 2001). Halogen bonding seems unlikely to cause the pre-edge feature because the predicted proportion of halogen molecules in the gas and solution are low. However, if the aqueous solution is

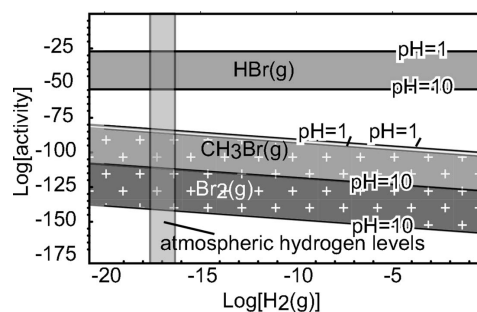


Figure 5

Maximum activity ranges for Br₂(g), CH₃Br(g) and HBr(g) in the fluid inclusion at room temperature. Activities are approximately equal to the mole fraction in the gas. The vertical bar indicates atmospheric hydrogen levels. Aqueous concentrations of Br₂, CH₃Br and HBr are likely to be less than the gaseous concentrations, so it is unlikely that much Br was hosted by these compounds in the SFLINCS at room temperature and pressure.

significantly affected by the presence of the CO_2 then the calculations could be wrong.

It is also useful to consider the inter-related effects of pH and speciation of the dissolved CO_2 . If heating causes changes in the distribution of CO_2 -bearing species and pH then this could affect the probability of the formation of intermolecular bonding. At room temperature the liquid in the SFLINCS is in equilibrium with an effectively pure CO_2 vapour phase, and the partial pressure, which is determined by the density of the SFLINC, is around 0.8 atmospheres. The pH within the SFLINC is determined by equilibrium with CO_2 , in the absence of other acids or bases, and is around 4. At this pH the CO_2 in the liquid will be present mostly as dissolved CO_2 with some associated carbonic acid. These CO_2 -bearing species would be more conducive to the type of electron distribution involved in intermolecular bonding than charged species, as intermolecular bonding requires partial electron transfer, a process which is already at completion in the charged species. The inability of CO_3^{2-} to participate in such bonding is consistent with the lack of a pre-edge feature for the CO_3^{2-} -saturated standard solutions. Increasing temperature increases pK values for CO_2 while temperature-induced decreases in hydrogen bonding favours increased ion association. These changes are unlikely to result in increased CO_2 dissociation, so the dominant species will continue to be CO_2 and H_2CO_3 . Changes in speciation are therefore unlikely to be a significant cause of the changes that result in the appearance and disappearance of the pre-edge feature.

Further experiments could provide more information on these alternatives. Laser Raman analysis would provide a more sensitive test than IR spectroscopy for the presence or absence of Br-bearing hydrocarbons, Br_2 and HBr. Laser Raman and/or NMR (nuclear magnetic resonance) spectroscopy could be used to investigate the extent of hydrogen bonding as a function of the CO_2 content of solution. Molecular simulations might also provide useful information.

4.5. Implications

The implication of this work, regardless of the precise cause of the Br edge, is that Br behaviour is different in CO_2 -bearing solutions to CO_2 -free solutions for a reason that is not accounted for by our current understanding of solution chemistry. Br in CO_2 -bearing solutions may then behave differently to Br in CO_2 -free solutions during processes such as phase separation and mineral crystallization. If Cl behaves similarly to Br then there are significant geological implications as Cl is an important complexing ligand for metals such as Cu, Zn and Ag (*e.g.* Liu *et al.*, 2001), so factors that influence its behaviour could also affect the transport and deposition of metals in solution. Studies of hydrothermal fluid–rock interactions are often forced to propose infiltration of multiple fluids from different sources (*e.g.* Bateman & Hagemann, 2004) because of the differing effects of fluid–rock interactions that can be observed at different locations within a fluid–rock system, or because of the apparent changes in fluid composition with time that are implied by superimposed

records of fluids in a single location. Consideration of CO_2 -related changes in fluid composition could help to reconcile these observations. Conventional thermodynamic calculations based on assumptions appropriate for H_2O -rich solvents do not predict the phenomena that may have caused the pre-edge feature. Thus, such calculations on CO_2 -rich fluids should be undertaken with care.

5. Conclusions

Br in CO_2 -bearing solutions exhibits a strong pre-edge feature at temperatures from 298 to 423 K. The feature becomes smaller and disappears as temperature increases, but reappears when temperature is reduced. The size of the feature increases as the proportion of CO_2 in the fluid inclusion increases. The distance between the first two post-edge maxima in the XANES is related to $X(\text{CO}_2)$. This is attributed to a CO_2 -related decrease in the polarity of the solvent.

Electronegativity considerations combined with knowledge of the system components suggest that covalent bonds capable of causing the pre-edge peak are H–Br, C–Br and Br–Br. Thermodynamic analysis suggests that reduced compounds are favoured by equilibration with Ni/NiO at high temperature, but calculations for lower temperatures suggest that the concentration of HBr(g), CH_3Br (g) and Br_2 (g) are vanishingly small and that the dominant Br-bearing species is the Br^- ion. An alternative possibility is that CO_2 affects the hydrogen-bonding network of water sufficiently that the systematics of anion hydration change, with a consequent change in the charge density around the Br^- ion that facilitates the electron transition thought to cause the pre-edge feature. Intermolecular bonding may also affect the charge density around Br^- ions. The presence of CO_2 causes halogen-bearing solutions to behave in ways that were previously unknown, with potentially significant consequences for the transport and deposition of metals in solution, for the consequences of phase separation and fluid–rock interaction.

The authors are grateful to two reviewers for reviews that improved the text. Use of the Advanced Photon Source was supported by the US Department of Energy, Office of Science, Office of Basic Energy Sciences, under Contract No. DE-AC02-06CH11357. This work was performed at GeoSoil-Enviro CARS (GSECARS), Sector 13, Advanced Photon Source at Argonne National Laboratory. The GSECARS is supported by the National Science Foundation – Earth Sciences, Department of Energy – Geosciences, W. M. Keck Foundation, and the USDA. KAE is supported by an Australian Synchrotron Research Program Fellowship and the work was further supported by the Australian Synchrotron Research Program, which is funded by the Commonwealth of Australia under the Major National Research Facilities Program.

References

- Ascone, I., D'Angelo, P. & Pavel, N. V. (1994). *J. Phys. Chem.* **98**, 2982–2990.

- Bateman, R. & Hagemann, S. (2004). *Min. Dep.* **39**, 536–559.
- Bodnar, R. J. (1994). *Geochim. Cosmochim. Acta*, **58**, 1053–1063.
- Brownlow, A. H. (1979). *Geochemistry*. New Jersey: Prentice Hall.
- Burattini, E., Dangelo, P., Giglio, E. & Pavel, N. V. (1991). *J. Phys. Chem.* **95**, 7880–7886.
- Chou, I. M., Eugster, H. P., Berens, P. & Weare, J. H. (1978). *Geochim. Cosmochim. Acta*, **42**, 281–288.
- D'Angelo, P., Di Cicco, A., Filipponi, A. & Pavel, N. V. (1993). *Phys. Rev. A*, **47**, 2055–2063.
- Di Cicco, A., Taglienti, M., Minicucci, M. & Filipponi, A. (2000). *Phys. Rev. B*, **62**, 12001–12013.
- Evans, K. A. (2006). *Geology*, **34**, 489–492.
- Feiters, M. C., Kupper, F. C. & Meyer-Klaucke, W. (2005). *J. Synchrotron Rad.* **12**, 85–93.
- Ferlat, G., San Miguel, A., Jal, J. F., Soetens, J. C., Bopp, P. A., Hazeman, J. L., Testemale, D. & Daniel, I. (2002). *J. Mol. Liq.* **101**, 127–136.
- Filipponi, A. & D'Angelo, P. D. (1998). *J. Chem. Phys.* **109**, 5356–5362.
- Filipponi, A., De Panfilis, S., Oliva, C., Ricci, M. A., D'Angelo, P. & Bowron, D. T. (2003). *Phys. Rev. Lett.* **91**, 165505.
- Fulton, J. L., Pfund, D. M., Wallen, S. L., Newville, M., Stern, E. A. & Ma, Y. (1996). *J. Chem. Phys.* **105**, 2161–2166.
- Fyfe, W. S., Price, N. J. & Thompson, A. B. (1978). *Fluids in the Earth's Crust*. Amsterdam: Elsevier.
- Grossfield, A. (2005). *J. Chem. Phys.* **122**, 02456–02452; 02456–02410.
- Jorgensen, W. L. & Madura, J. D. (1985). *Mol. Phys.* **56**, 1381–1392.
- Levason, W., Ogden, S. J., Spicer, M. D. & Young, N. A. (1990). *J. Chem. Soc. Dalton Trans.* **112**, 349–353.
- Lide, D. (2000). Editor. *Handbook of Chemistry and Physics*. Cleveland, OH: CRC Press.
- Liu, W. H., McPhail, D. C. & Brugger, J. (2001). *Geochim. Cosmochim. Acta*, **65**, 2937–2948.
- Matthews, W., Linnen R. L. & Guo Q. (2003). *Am. Mineral.* **88**, 701–707.
- Metrangolo, P., Neukirch, H., Pilati, T. & Resnati, G. (2005). *Acc. Chem. Res.* **38**, 386–395.
- Metrangolo, P. & Resnati, G. (2001). *Chem. Eur. J.* **7**, 2511–2519.
- Ravel, B. & Newville, M. (2005). *J. Synchrotron Rad.* **12**, 537–541.
- Shvarov, Y. & Bastrakov, E. (1999). *HCh: A Software Package for Geochemical Equilibrium Modelling. User's Guide*. Australian Geological Survey Organization, Canberra, Australia.
- Sterner, S. M. & Bodnar, R. J. (1991). *Am. J. Sci.* **291**, 1–54.
- Wallen, S. L., Palmer, B. J., Pfund, D. M., Fulton, J. L., Newville, M., Ma, Y. J. & Stern, E. A. (1997). *J. Phys. Chem. A*, **101**, 9632–9640.
- Walther, J. V. (1992). *J. Met. Geol.* **10**, 789–797.